

See discussions, stats, and author profiles for this publication at: <https://www.researchgate.net/publication/231646669>

Why Does Gold(III) Porphyrin Act as a Selective Catalyst in the Cycloisomerization of Allenones?

ARTICLE *in* THE JOURNAL OF PHYSICAL CHEMISTRY C · DECEMBER 2010

Impact Factor: 4.77 · DOI: 10.1021/jp1101384

CITATIONS

19

READS

51

3 AUTHORS:



A. Nijamudheen

University at Buffalo, The State University of...

26 PUBLICATIONS 173 CITATIONS

[SEE PROFILE](#)



Deepthi Jose

Ecole Centrale de Lyon

14 PUBLICATIONS 282 CITATIONS

[SEE PROFILE](#)



Ayan Datta

Indian Association for the Cultivation of Scie...

96 PUBLICATIONS 1,487 CITATIONS

[SEE PROFILE](#)

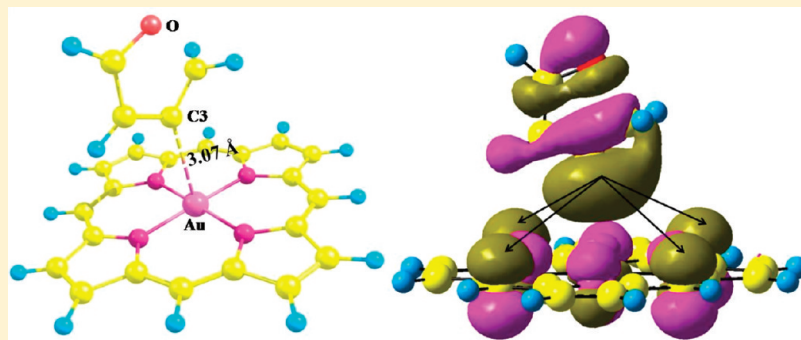
Why Does Gold(III) Porphyrin Act as a Selective Catalyst in the Cycloisomerization of Allenones?

A. Nijamudheen, Deepthi Jose, and Ayan Datta*

School of Chemistry, Indian Institute of Science Education and Research Thiruvananthapuram, CET Campus, Thiruvananthapuram-695016, Kerala 23362, India

Supporting Information

ABSTRACT: The chemical basis (electronic and steric factors) through which $[\text{Au}(\text{TPP})]\text{Cl}$ acts as a highly efficient chemoselective catalyst (even more than other homogeneous Au(III) catalysts like AuCl_3 and $[\text{Au}(\text{salen})]\text{Cl}$) in the conversion of allenone to furan is elucidated. The planar aromatic structure of porphyrin unit stabilizes the transition state for ring closure through symmetric orbital interactions between allenone and the catalyst to create a lower energy cyclization pathway. Even though AuCl_3 catalyzes the cyclization of allenone very efficiently, the inability for the reaction to terminate and the possibility for further reactions that lead to oligomerization of allenone through new C–C bond formation reduce its synthetic utility. A detailed mechanistic investigation on the dimerization of allenone in the presence of AuCl_3 provides a theoretical rationale for the previous experimental results. In the case of the $[\text{Au}(\text{salen})]^+$ -catalyzed reaction, the higher activation energy required to cross the barrier for cyclization reduces its efficiency.

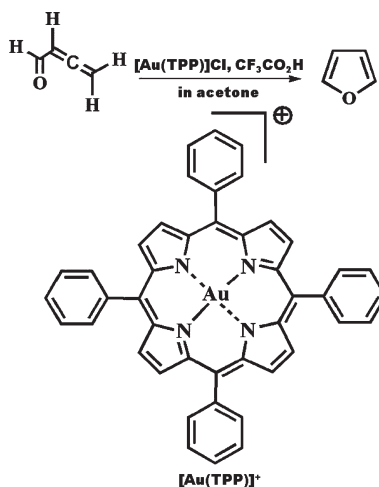


INTRODUCTION

Homogeneous catalysis by gold complexes is becoming increasingly popular for the formation of C–C, C–N, C–S, and C–O bonds in organic transformations.^{1–16} Gold catalysts are being actively and very efficiently utilized for the cyclization of alkynes and allenes.^{17–22} Lewis acid catalysts like AuCl_3 or AuPPh_3Cl are now routinely utilized for such transformations.^{23–31} However, the major goal in the area of catalysis by Au-salts is to develop very efficient as well as chemoselective reagents with high catalytic turnovers. In this context, metalloporphyrin-mediated functionalization of hydrocarbons has been very effective for organic and biomimetic studies.^{32–37} The presence of the porphyrin ring provides an innovative means to fine-tune the steric and electronic requirements of the reactions and thus leads to very selective product formation. Che and co-workers have shown excellent conversion of allenones (~98%) into furans using Au–tetraphenylporphyrin chloride ($[\text{Au}(\text{TPP})]\text{Cl}$) (see Scheme 1).³⁸ The specificity of this complex was understood on the basis of much lower efficiency and formation of other side products for the same reaction performed with $[\text{Au}(\text{salen})]\text{Cl}$, salen = N,N' -ethylenebis(salicylimine), and AuCl_3 , respectively. However, the molecular origin for such high specificity of catalysis in $[\text{Au}(\text{TPP})]\text{Cl}$ is not clearly understood, and a detailed mechanistic study based on DFT calculations is performed in this Article to explain the high activity of the porphyrin coordinated Au(III) complex.

We have considered the presence of counterion and solvent in the reaction profile and found that the proton donor, trifluoroacetic

Scheme 1. Cycloisomerization of Allenone Catalyzed by $[\text{Au}(\text{TPP})]^+$ (From Ref 38)



acid (TFA), acts as a cocatalyst in these transformations. Such mechanistic understanding of cycloisomerization and dimerization³⁹ of allenones in the presence of homogeneous Au(III) catalysts

Received: October 22, 2010

Revised: December 9, 2010

Published: December 30, 2010

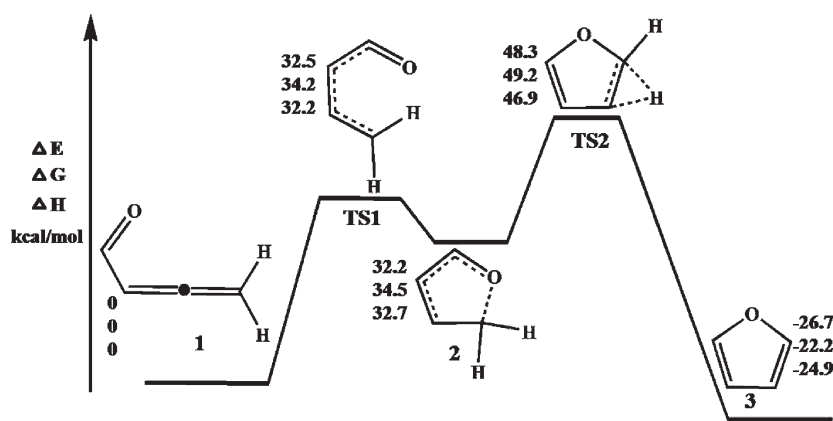


Figure 1. Potential energy profile computed for conversion of allenone into furan in the absence of any catalyst (gas-phase calculations using B3LYP/6-31G(d) level of theory).

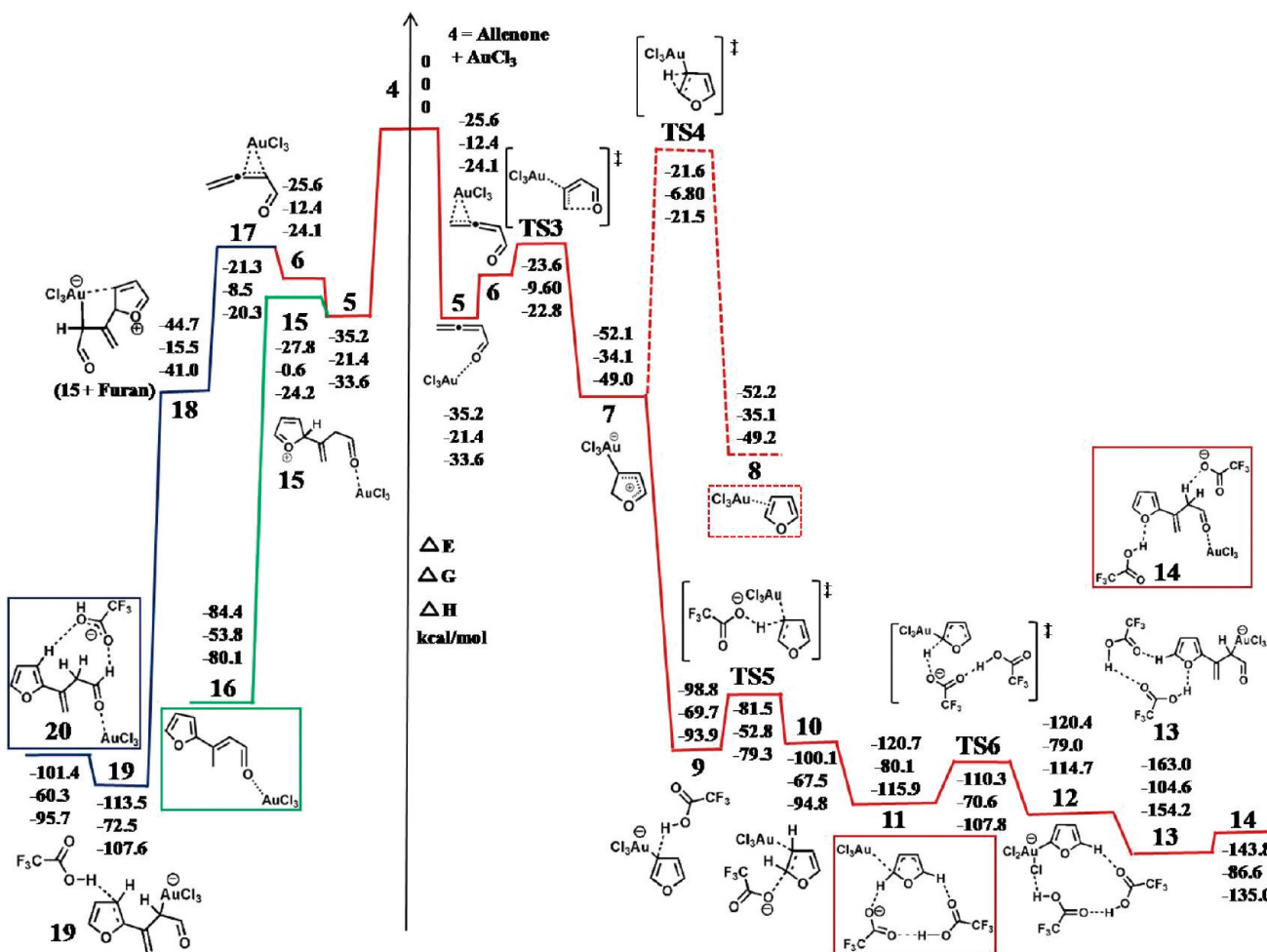


Figure 2. Potential energy profile computed for conversion of allenone into furan in the presence of AuCl_3 and $\text{CF}_3\text{CO}_2\text{H}$ (gas-phase calculations using B3LYP/LANL2DZ level of theory).

can provide useful insights for designing new organic synthetic strategies based on these catalysts.

COMPUTATIONAL METHODS

$[\text{Au}(\text{porphyrin})]^+$ complex is chosen as a model for $[\text{Au}(\text{TPP})]\text{Cl}$ in the present study. All the calculations reported have

been performed using the Gaussian 03 suite of programs.⁴⁰ The structures of the molecules, complexes, intermediates, and the transition states are optimized via the DFT method using the B3LYP hybrid functional theory.^{41,42} Los Alamos 19 electron shape consistent relativistic ECP (LANL2DZ) basis set⁴³ was used for all the structures reported for the gold-catalyzed

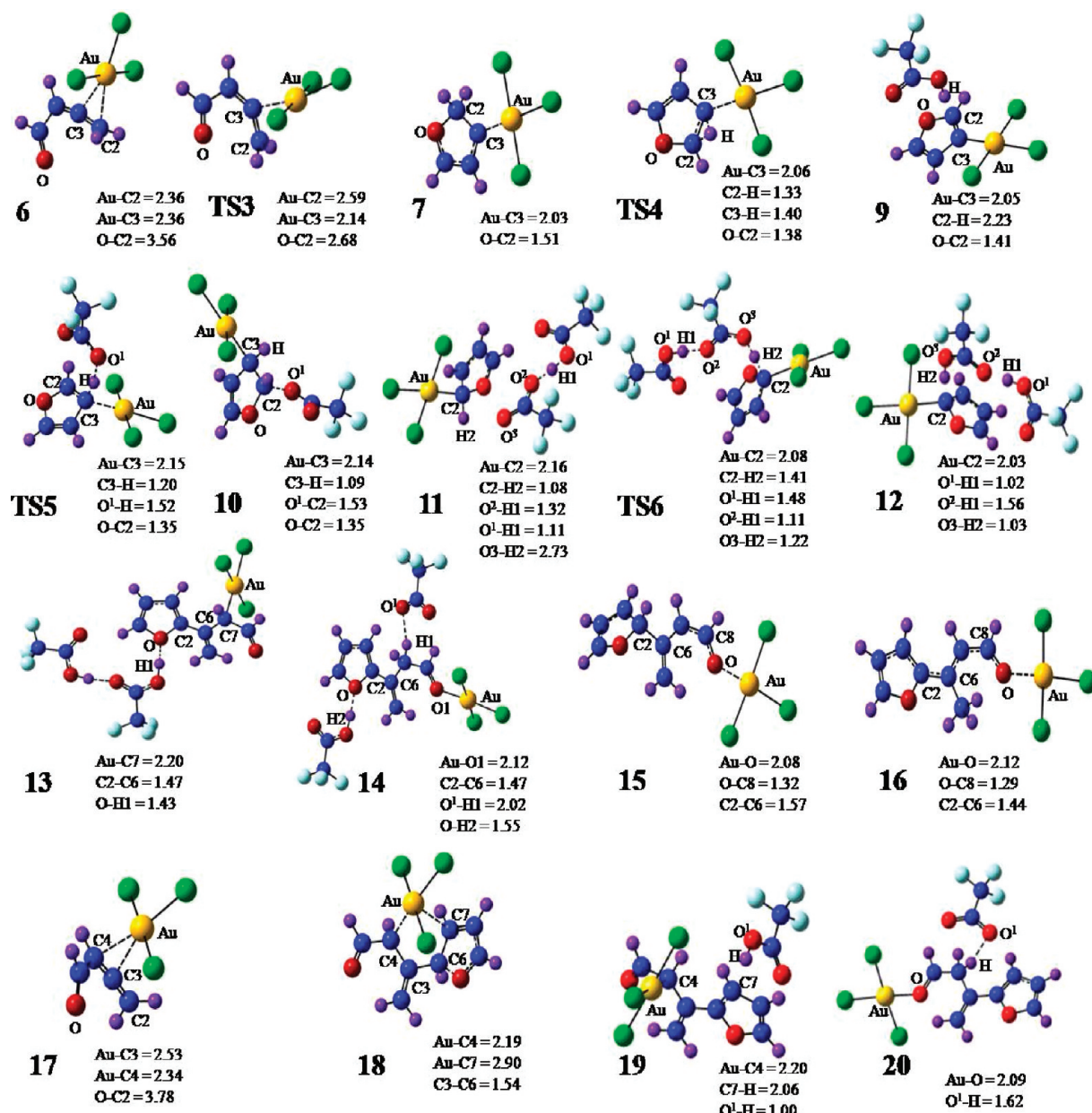


Figure 3. Geometries of the intermediates and transition states computed for the AuCl_3 -catalyzed reaction (shown in Figure 2) with selected distances in angstroms.

reactions. The 6-31G(d) basis set⁴⁴ was used to optimize all the structures reported for the uncatalyzed cycloisomerization of allenone (shown in Figure 1). These structures were also optimized using LANL2DZ basis set to find out the binding energies/relative energies of the complexes, intermediates, and transition states reported for the gold-catalyzed reactions. For the $[\text{Au}(\text{porphyrin})]^+$ -catalyzed reaction, additional calculations were performed using a split basis set method with 6-31G(d) basis set for main group elements and LANL2DZ basis set for Au atom. Comparable results were obtained for the calculations with different basis sets (see the Supporting Information). All the structure calculations were followed by vibrational analyses to ensure all positive frequencies for the ground states and intermediates and one imaginary frequency for the transition states. All the thermo-chemical calculations are reported at 298 K.

The relative energies of the structures shown for the gold-catalyzed reactions were calculated as $\Delta E = \text{energy of the structure} - \text{sum of the energies of individual reactants}$. Basis set super position error (BSSE) can effect the binding energies/relative energies of individual structures discussed in this Article.⁴⁵ For example, the BSSE corrected and the BSSE uncorrected binding energies of structure 5 shown in Figure 2 are of $\Delta E = -35.2$ and -29.9 kcal/mol, respectively. However, the BSSE correction does not change the barriers significantly because the similar values of BSSE correction for the ground states and the barriers will cancel each other when considering their difference. Hence, only the BSSC uncorrected energies are discussed here (see the Supporting Information for BSSE corrected values). All the solvent calculations were done by using the Self Consistent Reaction Field (SCRF)⁴⁶ method with the Polarizable

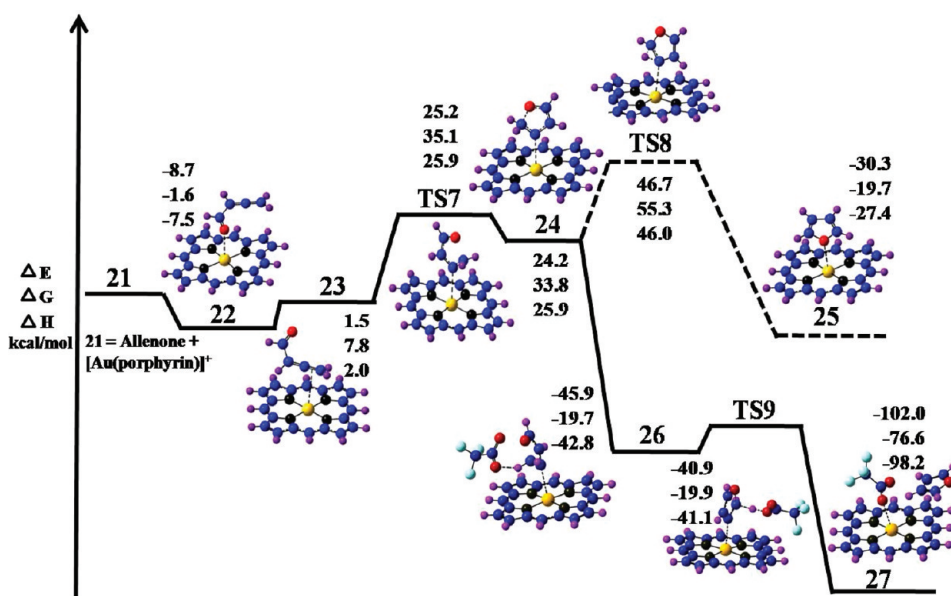
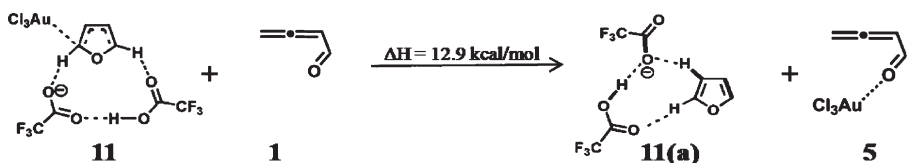


Figure 4. Potential energy profile computed for conversion of allenone into furan in the presence of $[\text{Au}(\text{porphyrin})]^+$ and $\text{CF}_3\text{CO}_2\text{H}$ (gas-phase calculations using B3LYP/LANL2DZ level of theory; see also Figure 5).

Scheme 2. Formation of Product 11(a) from 11



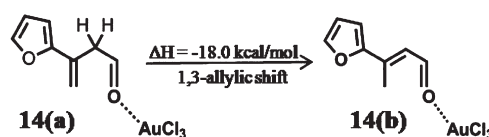
Continuum Model (PCM)⁴⁷ using the United Atom Topological Model for generating the radii (radii = UAKS)⁴⁸ as implemented in the Gaussian 03 program package.

RESULTS AND DISCUSSION

As shown in Figure 1, the conversion of allenone (1)^{49,50} into furan (3) (exothermicity, $\Delta H^\ddagger = -24.9 \text{ kcal/mol}$) involves crossing two different barriers, one wherein the $\text{C}=\text{C}=\text{C}$ bonds bend to accommodate cyclization (TS1) and the other being a H-shift between the adjacent carbon atoms (TS2). These two barriers are connected by a cyclic intermediate (2) with a long C–O bond (1.56 Å). C_s symmetry for 2 ensures equal migratory aptitude for either of the two H atoms. The very large barrier height of $\Delta H^\ddagger = 32.2 \text{ kcal/mol}$ for bending explains the non feasibility of the reaction in the absence of catalysts. Calculations including acetone as a solvent at SCRF level lead to inconsequential changes in the barrier heights ($\Delta H^\ddagger = 31.8 \text{ kcal/mol}$ for TS1 and $\Delta H^\ddagger = 13.9 \text{ kcal/mol}$ for TS2).

To understand the effect of the presence of Au(III) on the cyclization of allenone, the reaction was studied in the presence of AuCl_3 . The potential energy profile calculated for the AuCl_3 -catalyzed cycloisomerization in the gas phase is shown in Figure 2. AuCl_3 exists as a Cl-bridged dimer, Au_2Cl_6 (D_{2h} symmetry),^{51,52} and its dissociation, $\text{Au}_2\text{Cl}_6 \rightarrow 2\text{AuCl}_3$, is highly endothermic ($\Delta H = 49.3 \text{ kcal/mol}$). The endothermicity is partly compensated by the formation of an exothermic oxophilic allenone \cdots AuCl_3 complex (5) ($\Delta H = -33.6 \text{ kcal/mol}$ in gas phase, -35.4 kcal/mol in acetone). The stability of 5 is understood on the basis

Scheme 3. Isomerization of the $\text{Au}\cdots\cdots\text{Dimer } 14(\text{a})$ to $14(\text{b})$



of the formation of a σ -complex between allenone and AuCl_3 through the interaction of the lone pair of electrons on the carbonyl oxygen and the electron-deficient Au atom in AuCl_3 (short $\text{Au}\cdots\cdots\text{O}=\text{C}$ distance of 2.11 Å). However, before the ring closure (through TS3) for the formation of 7, the allenone undergoes a crossover from the oxophilic complex (5) to the π -philic intermediate (6), with substantial interaction of the π -electrons of the $-\text{CH}=\text{CH}_2$ with AuCl_3 . Formation of such a π -complex is in agreement with previous experimental and computational studies on ring closure of allenones.^{38,53–55} The ring-closed intermediate (7) undergoes a 1,2 hydride shift from the adjacent carbon (see the structure, TS4) to form furan in 8. The barrier height (ΔH^\ddagger) for the β -H elimination process is 27.5 kcal/mol. It is interesting to note that even though the structure of 7 is non symmetric and as a result of which the migratory aptitudes for the two H-atoms on the ring are expected to differ, the distances between each of the two H-atoms and the Au-atom in AuCl_3 are of 3.45 and 3.46 Å. Thus, the barrier heights for the shift of both the H-atoms are almost equivalent (see the Supporting Information). Followed

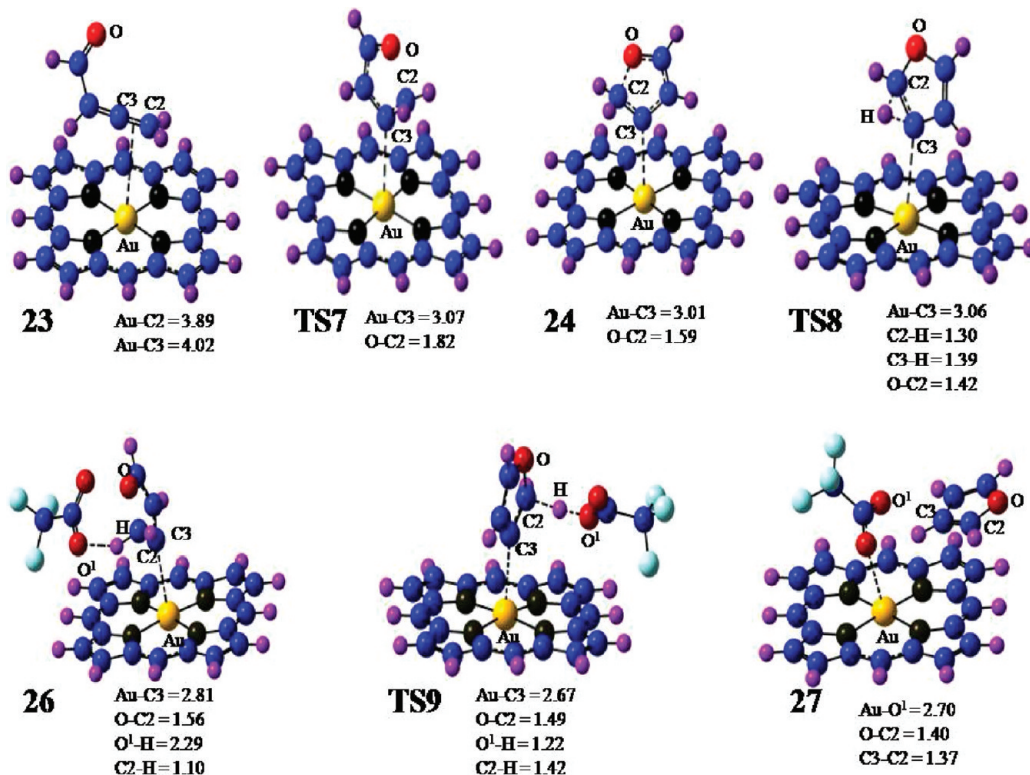


Figure 5. Geometries of transition states and intermediates for $[\text{Au}(\text{porphyrin})]^+$ -catalyzed reaction (shown in Figure 4) with selected distances in angstroms.

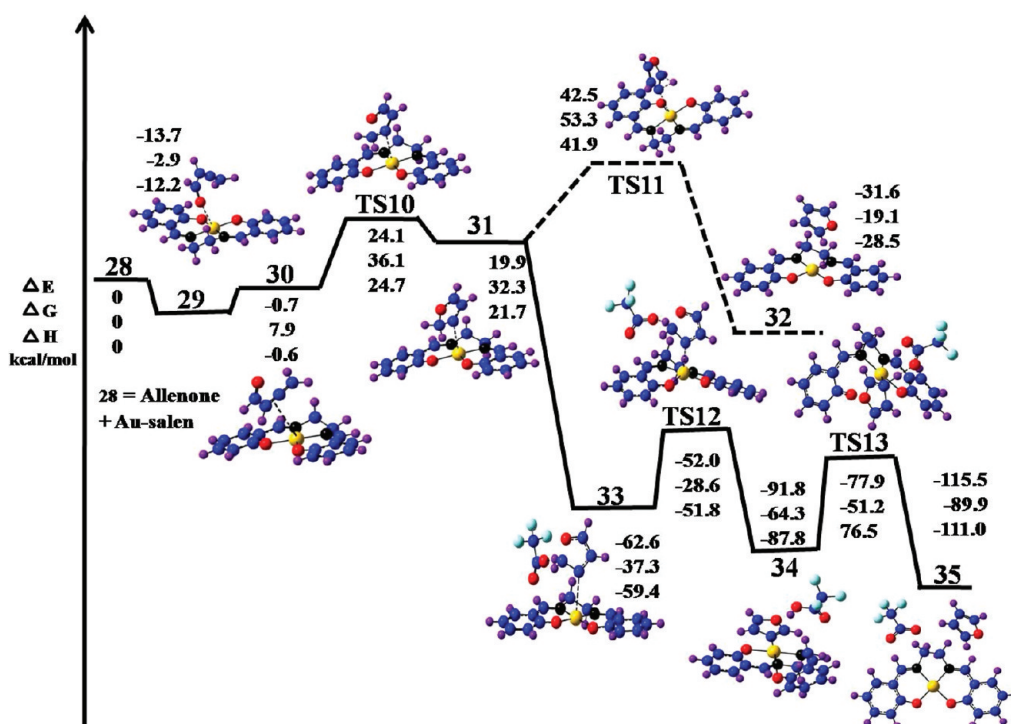


Figure 6. Potential energy profile computed for the conversion of allenone into furan in the presence of $[\text{Au}(\text{salen})]^+$ and $\text{CF}_3\text{CO}_2\text{H}$ (gas-phase calculations using B3LYP/LANL2DZ level of theory).

by the H-shift reaction that results in the formation of furan, a furan $\cdots\text{AuCl}_3$ complex (8) is formed through the interaction of the π -electrons of furan with AuCl_3 . The C=C bond elongates by $\sim 0.08 \text{ \AA}$ in the furan $\cdots\text{AuCl}_3$ complex in comparison to the

uncoordinated furan in the gas phase due to ligand to metal charge transfer (LMCT) from the molecule to AuCl_3 . A comparison of the computed mechanisms for the uncatalyzed reaction (Figure 1) and the AuCl_3 -catalyzed reaction (Figure 2)

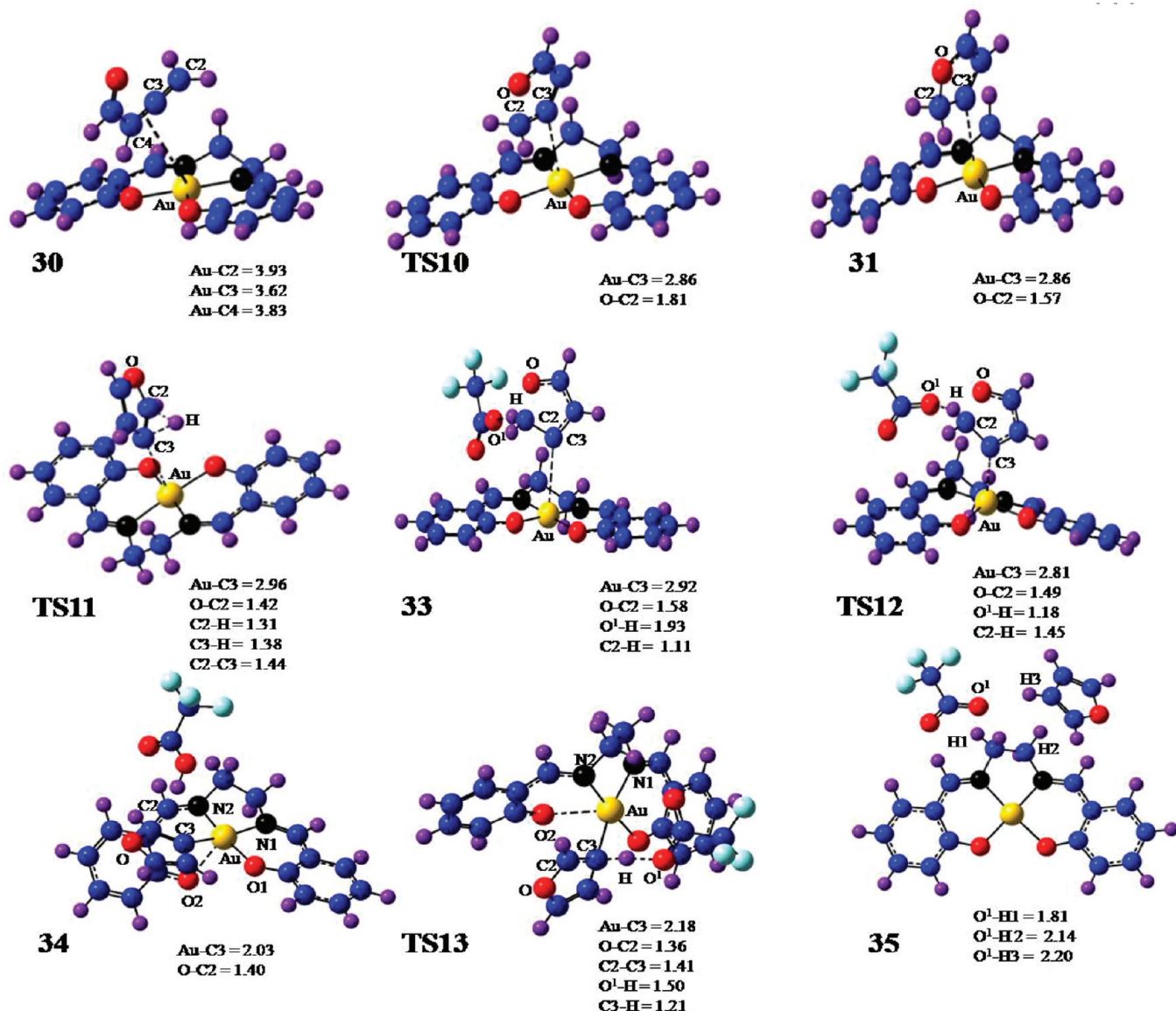


Figure 7. Geometries of transition states and intermediates for $[\text{Au}(\text{salen})]^+$ -catalyzed reaction (shown in Figure 6) with selected distances in angstroms.

shows that even though coordination of allenone with AuCl_3 reduces the barrier for angle closure and cyclization remarkably (from 32.2 to 1.3 kcal/mol), the barrier for the H-shift reaction increases significantly (from 14.2 to 27.5 kcal/mol). No profound changes from the gas-phase calculations were observed for the barriers computed in acetone at the SCRF level (see the Supporting Information). The above results are in good agreement with the previous experimental reports that β -H elimination of gold carbene intermediate is energetically unfavorable for most of the reactions involving homogeneous catalysis by gold.⁵⁶ The experimental study by Che et al. has shown that TFA is inevitable for the reaction, and it proceeds through deprotonation of 7 followed by a proto-demetalation step to furan.³⁸ Hence, we decided to model the reaction in the presence of TFA.⁵⁷

Our calculations reveal that CF_3CO_2^- abstracts a proton from the C2 of intermediate 7 through a barrierless transition state to form 9. Protonation of the gold carbene intermediate in 9 by

$\text{CF}_3\text{CO}_2\text{H}$ leads to 10 in which CF_3CO_2^- is complexed with the $\text{AuCl}_3 \cdots$ furan complex at C2 through a long C–O σ bond ($=1.53 \text{ \AA}$). The activation energy required for the CF_3CO_2^- assisted rearrangement of the intermediate 7 to 10 is just 14.6 kcal/mol as compared to 27.5 kcal/mol required for a hydride shift mechanism from 7 to 8 in the absence of TFA. The solvent calculations in acetone change the relative energies of charged species like 9 ($\Delta H = -70.8 \text{ kcal/mol}$ in the solvent phase), TSS ($\Delta H = -57.7 \text{ kcal/mol}$ in the solvent phase), etc., considerably. However, the barriers remain almost unchanged as compared to the values shown in Figure 2. For example, the energy required to cross the barrier TSS in the solvent phase is $\Delta H^\ddagger = 13.1 \text{ kcal/mol}$ against 14.6 kcal/mol in the gas phase. Protonation of CF_3CO_2^- in 10 by another molecule of TFA weakens the interaction between CF_3CO_2^- and the $\text{AuCl}_3 \cdots$ furan complex (11) (in 11, TFA and CF_3CO_2^- are bonded to the $\text{AuCl}_3 \cdots$ furan complex through weak H-bonding interactions as shown in Figure 3). The attack of another allenone molecule on this $\text{AuCl}_3 \cdots$ furan

complex results in the formation of furan weakly bonded to TFA and CF_3CO_2^- (**11(a)**) and **5** (Scheme 2). Removing AuCl_3 from **11** followed by its optimization leads to **11(a)**.

The plausible mechanism computed for the dimerization that occurs during this cyclization can be outlined as follows. The CF_3CO_2^- abstracts the H-atom on the C2 of furan in **11**, resulting in the furyl-gold species **12**. The reaction proceeds through the transition state **TS6** (with an energy barrier of 8.1 kcal/mol) corresponding to the hydrogen atom abstraction by CF_3CO_2^- . The Au–C bond length decreases from 2.16 Å in **11** to 2.03 Å in **12**, which is the typical gold carbene bond distance.^{58–60} A second molecule of allenone then undergoes a Michael addition⁶¹ with the furyl-gold species followed by migration of AuCl_3 from C2 to C7 to form **13**. The bond length of newly formed C–C σ bond between furan and allenone in **13** is 1.47 Å (C2–C6 of **13** in Figure 3). Our computation well agrees with the previous time-dependent proton NMR analysis by Hashmi et al.,³⁹ which has monitored the presence of the furyl-gold species **12**. A proto-demetalation process from the intermediate **13** assisted by TFA forms the dimer **14**. Actually, **14** is an oxophilic complex of the dimer and AuCl_3 , very much similar to **5**. In **14** the Au–O1 bond distance is of 2.12 Å, which is almost equal to the Au–O bond length in **5** (2.11 Å). It clearly indicates the possibilities for further reactions of the dimer leading to the formation of trimer and tetramer. Thus, a living polymerization mechanism as reported by Hashmi et al. is confirmed from our calculations.^{39,56} A 1,3-allylic shift from the dimer **14(a)** (Scheme 3) gives the thermodynamically more stable isomer **14(b)**. Exothermicity for the rearrangement is $\Delta H = -18.0$ kcal/mol.

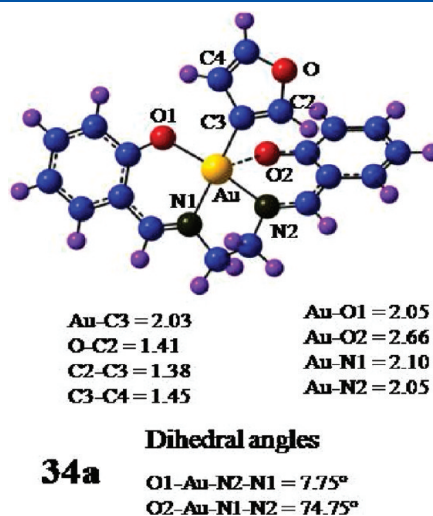


Figure 8. Geometry of the gold carbene intermediate in **34** with selected distances in angstroms and dihedral angles in degrees.

Alternative mechanisms studied for the dimerization of allenone catalyzed by AuCl_3 proceed through Michael addition between furan and allenone coordinated to AuCl_3 . Two reaction pathways starting with the furan molecule and allenones of different modes of coordination to AuCl_3 are shown on the left-hand side of Figure 2. According to the first mechanism, the oxophilic $\text{AuCl}_3 \cdots$ allenone complex **5** undergoes an electrophilic aromatic substitution on furan molecule to give the dimer through the formation of intermediate **15**. A rearrangement of this intermediate, assisted by the acid, leads to the $\text{AuCl}_3 \cdots$ dimer complex **16**. In the dimer, the newly formed C–C bond is shortened considerably (bond length = 1.44 Å) due to the extensive delocalization of π -electrons in the system. The Au–O bond distance increases from 2.08 Å in **15** to 2.12 Å in **16**. Exothermicity of the rearrangement of **15** to **16** is calculated to be $\Delta H = -54.4$ kcal/mol. The second mechanism for the dimerization from furan involves the conversion of **6** to its isomeric π -philic $\text{AuCl}_3 \cdots$ allenone intermediate **17** in which the Au-atom of the catalyst is coordinated to the sterically demanded double bond of allenone. Even though the formation of **17** ($\Delta H = 3.8$) from **6** is disfavored by 2.5 kcal/mol as compared to crossing the cyclization barrier **TS3**, the low endothermicity for the reaction and the stability of intermediate formed **18** ($\text{BE} = -23.4$ kcal/mol, $\text{BE} = E(\mathbf{18}) - E(\text{furan}) - E(\mathbf{17})$) make it a possible reaction path. The subsequent proton abstraction and proto-demetalation on **18** assisted by CF_3CO_2^- forms the $\text{AuCl}_3 \cdots$ dimer oxophilic complex (**20**). A comparison of the two mechanisms starting with furan and Au–allenone complexes shows that the 1,4 conjugate addition of **5** to furan constitutes energetically favorable reaction. However, the contribution from the second mechanism cannot be neglected completely due to the low barrier for the formation of **17** and the higher stability of **18**. On the basis of the above results, it can be concluded that AuCl_3 is a potent catalyst for the creation of a new C–C bond, and the most plausible mechanism of dimerization involves the formation of a gold-furyl species. Hence, it is not a promising candidate for the conversion of allenone to furan. However, suitably substituted allenone molecules can prevent the dimerization effectively. Gevorgyan et al. have used the strategy to synthesize substituted furans such as halofurans and silylfurans.^{23,24,53}

The potential energy profile computed for the conversion of allenone to furan in the presence of $[\text{Au}(\text{porphyrin})]^+$ is shown in Figure 4. The interaction of allenone with $[\text{Au}(\text{porphyrin})]^+$ is much weaker ($\Delta H = -7.5$ kcal/mol in the gas phase and -7.3 kcal/mol in acetone) than for AuCl_3 due to the poor Lewis acid nature of $[\text{Au}(\text{porphyrin})]^+$. The mode of interaction of allenone with the Au-atom is still through the lone pair of electrons on the oxygen end (long Au \cdots O=C distance of 2.91 Å). A poor Au \cdots O=C interaction ensures that reorganization of the mode of interaction from oxophilic contact (**22**) to the π -philic intermediate (**23**) involves a much smaller energy

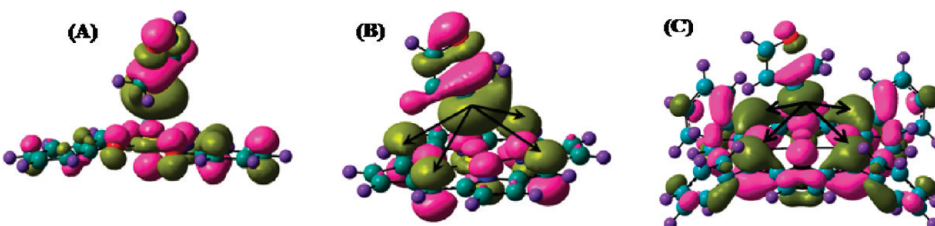


Figure 9. HOMO for the transition states: (A) **TS5** for $\text{Au}(\text{salen})^+$, (B) **TS7** for $\text{Au}(\text{porphyrin})^+$, and (C) **TS7** for the $[\text{Au}(\text{TPP})]^+$.

change ($\Delta H = 5.5$ kcal/mol in the gas phase and 4.2 kcal/mol in acetone) as compared to that with AuCl_3 . The π -philic reactive intermediate undergoes ring closure in **24** through **TS7** with a barrier height, $\Delta H^\ddagger = 23.9$ kcal/mol. A β -H elimination of **24** (through **TS8**, $\Delta H^\ddagger = 20.1$ kcal/mol) forms furan that exists as a complex with $[\text{Au}(\text{porphyrin})]^+$ through the interaction of the lone pair of electrons of the oxygen of furan with the planar $[\text{Au}(\text{porphyrin})]^+$ unit along the axial end to form a square pyramidal structure rather than a π -complex. The coordination of $[\text{Au}(\text{porphyrin})]^+$ with allenone reduces the barrier for cyclization as compared to the uncatalyzed reaction by 8.3 kcal/mol (**TS1** vs **TS7**), but the barrier height for H-shift is higher than the uncatalyzed one (**TS2** vs **TS8**). Next, we explored the effect of counterion on the rearrangement of cyclic allenone intermediate in **24**. CF_3CO_2^- forms a H-bond (2.3 Å) with the intermediate **24** through the interaction of O-atom in CF_3CO_2^- with one of the C2 hydrogen atoms of cyclic allenone to form **26**. A proto-demetalation process from **26** through the barrier **TS9** leads to the formation of furan and the $\text{CF}_3\text{CO}_2^- \cdots$ catalyst complex (see the structure **27**). Very interestingly, no formation of gold carbene intermediate typical for the homogeneous Au-catalysis was observed, and the barrier for proto-demetalation is just 1.7 kcal/mol. The steric bulk of the catalyst $[\text{Au}(\text{porphyrin})]^+$ rules out the possibility for the dimerization.

To understand the effect of bulkiness of the ligand, we have also modeled the reaction in the presence of $[\text{Au}(\text{salen})]^+$.^{59,60} In the absence of TFA, the potential energy profile is very much similar to that of the $[\text{Au}(\text{porphyrin})]^+$ -catalyzed reaction (see Figure 6). The π -philic reactive intermediate undergoes ring closure in **31** through **TS10** with a barrier height of $\Delta H^\ddagger = 25.3$ kcal/mol. A H-shift reaction from C2 to C3 of **31** (through **TS11**, $\Delta H^\ddagger = 20.2$ kcal/mol) forms furan that exists as a complex with $[\text{Au}(\text{salen})]^+$ via the facial aromatic π -electrons (binding energy of the furan \cdots catalyst complex (**32**) $\Delta E = -4.8$ kcal/mol with respect to the energy of salen and furan). Similar to $[\text{Au}(\text{porphyrin})]^+$ catalyst, the barrier for cyclization is low as compared to that for the uncatalyzed reaction by 6.9 kcal/mol (**TS1** vs **TS10**). Yet the barrier height for H-shift still remains much higher (**TS2** vs **TS11**). In the presence of TFA, the proto-demetalation process occurs by crossing two different barriers.^{62,63}

A proton abstraction from the intermediate **33** through the barrier **TS12** ($\Delta H^\ddagger = 7.6$) leads to the gold carbene intermediate in **34** in which the deprotonated cyclic allenone species forms a complex with the catalyst through a C–Au bond of 2.03 Å (Figure 7). In **34a** (the geometry of **34** without showing the CF_3CO_2^-), the strong C–Au bond weakens one of the two O–Au bonds of the catalyst (bond length increases from 2.04 to 2.66 Å), hence deforming its pseudoplanar structure (see Figure 8). A proto-demetalation step from **34** through the barrier **TS13** ($\Delta H^\ddagger = 11.3$ kcal/mol) leads to the formation of furan and a $\text{CF}_3\text{CO}_2^- \cdots [\text{Au}(\text{salen})]^+$ complex.

To critically understand the origin of the stability of the transition state for cyclization of allenone with $[\text{Au}(\text{porphyrin})]^+$, a molecular orbital analysis was performed for **TS7** and **TS10**. The HOMOs for the two systems are shown in Figure 9. While the $[\text{Au}(\text{salen})]^+$ complex with allenone shows no orbital interactions, in-phase interactions between the four nonpyrrole sp^2 carbons and the cyclic allenone are evident in the **TS7**. Thus, electronic interactions available due to the planar aromatic structure in porphyrin lower the barrier height for cyclization in allenone. Also, apart from the low barrier height in **TS7**, the low reorganization energy associated with the formation of the

π -philic reactive intermediate (**13**) from the loosely bound oxophilic complex (**12**) facilitates the pathway for allenone to furan conversion in the presence of $[\text{Au}(\text{porphyrin})]^+$ moiety. Such orbital interactions were confirmed for the computation performed with the $[\text{Au}(\text{TPP})]^+$ catalyst (Figure 9C).

CONCLUSIONS

The present computation explains the catalytic activity of the Au–porphyrin complex in the conversion of allenone to furan. The ability of porphyrin complex to reduce the barrier for cyclization arises primarily due to its π -conjugated planar aromatic structure, which facilitates electronic stabilization of the transition state. Also, bulkiness of the porphyrin ligand favors a fast proto-demetalation process in the presence of CF_3CO_2^- . The role of TFA as a cocatalyst is understood on the basis of a much higher activation energy required for the β -H elimination of the gold-cyclic allenone intermediate in its absence. Surprisingly, gold carbene intermediate formation typical for the gold-catalyzed cycloisomerization of allenone was not found for the Au–porphyrin reaction. Even though $[\text{Au}(\text{salen})]^+$ can activate the allene double bond toward cyclization, higher barriers of energy corresponding to the cyclization and proto-demetalation processes make it less efficient than $[\text{Au}(\text{porphyrin})]^+$ for the reaction. Therefore, it is the electronic reasons rather than the steric factors that make $[\text{Au}(\text{porphyrin})]^+$ a highly efficient catalyst. Mechanisms for the cycloisomerization and dimerization of allenone in the presence of AuCl_3 and TFA were investigated in detail. The most plausible mechanism for the dimerization is found to be the one that involves the formation of a gold substituted furan. Even though AuCl_3 is a better Lewis acid catalyst for the cycloisomerization of allenone, our computation confirms the previous experimental results that further reactions activated by AuCl_3 lead to C–C bond formation, resulting in the dimerization of the allenone that reduces the yield of furan.

ASSOCIATED CONTENT

S Supporting Information. Cartesian coordinates, energies, harmonic frequencies for all the structures reported, additional calculations, and complete ref 40. This material is available free of charge via the Internet at <http://pubs.acs.org>.

AUTHOR INFORMATION

Corresponding Author

*E-mail: ayan@iisertvm.ac.in.

ACKNOWLEDGMENT

A.D. and A.N. thank DST-fast Track Scheme (Government of India) and CSIR for partial research funding. D.J. thanks CSIR for JRF.

REFERENCES

- (1) Bhaduri, S.; Mukesh, D. *Homogeneous Catalysis: Mechanisms and Industrial Applications*; Wiley-Interscience: New York, 2000.
- (2) Heaton, B. *Mechanisms in Homogeneous Catalysis: A Spectroscopic Approach*; Wiley-VCH: New York, 2005.
- (3) Hashmi, A. S. K. *Gold Bull.* **2004**, 37/1–2, 51.
- (4) Anja, H.-R.; Norbert, K. *Org. Biomol. Chem.* **2005**, 3, 387.
- (5) Gorin, D. J.; Sherry, B. D.; Toste, F. D. *Chem. Rev.* **2008**, 108, 3351.
- (6) Morita, N.; Krause, N. *Angew. Chem., Int. Ed.* **2006**, 45, 1897.

- (7) Bond, G. C.; Louis, C.; Thompson, D. T. *Catalysis by Gold*; Imperial College Press: London, UK, 2006.
- (8) Lalonde, R. L.; Wang, J. Z.; MBA, M.; Lackner, A. D.; Toste, F. D. *Angew. Chem., Int. Ed.* **2010**, *49*, 598.
- (9) Li, Y.; Zhou, F.; Forsyth, C. J. *Angew. Chem., Int. Ed.* **2007**, *46*, 279.
- (10) de Haro, T.; Nevado, C. *J. Am. Chem. Soc.* **2010**, *132*, 1512.
- (11) Yamamoto, Y.; Gridnev, I. D.; Patil, N. T.; Jin, T. *Chem. Commun.* **2009**, 5075.
- (12) Hashmi, A. S. K.; Blanco, M. C.; Fischer, D.; Bats, J. W. *Eur. J. Org. Chem.* **2006**, 1387.
- (13) Patil, N. T.; Konala, A.; Singh, V.; Reddy, V. V. N. *Eur. J. Org. Chem.* **2009**, 5178.
- (14) Patil, N. T.; Kavthe, R. D.; Raut, V. S.; Shinde, V. S.; Sridhar, B. *J. Org. Chem.* **2010**, *75*, 1277.
- (15) Li, Y.; Zhou, F.; Forsyth, C. J. *Angew. Chem., Int. Ed.* **2007**, *46*, 279.
- (16) Patil, N. T.; Raut, V. S.; Kavthe, R. D.; Reddy, V. V. N.; Raju, P. V. K. *Tetrahedron Lett.* **2009**, *50*, 6576.
- (17) Kleinbeck, F.; Toste, F. D. *J. Am. Chem. Soc.* **2009**, *131*, 9178.
- (18) Kovacs, G.; Ujaque, G.; Lledos, A. *J. Am. Chem. Soc.* **2008**, *130*, 853.
- (19) Nijamudheen, A.; Datta, A. *J. Mol. Struct. (THEOCHEM)* **2010**, *945*, 93.
- (20) Mohan, P. J.; Datta, A.; Mallajosyula, S. M.; Pati, S. K. *J. Phys. Chem. B* **2006**, *110*, 18661.
- (21) Patil, N. T.; Singh, V.; Konala, A.; Mutiyala, A. K. *Tetrahedron Lett.* **2010**, *51*, 1493.
- (22) Kinder, R. E.; Zhang, Z.; Widenhoefer, R. A. *Org. Lett.* **2008**, *10*, 3157.
- (23) Sromekaw, A. W.; Rubina, M.; Gevorgyan, V. *J. Am. Chem. Soc.* **2005**, *127*, 10500.
- (24) Xia, Y.; Dudnik, A. S.; Gevorgyan, V.; Li, Y. *J. Am. Chem. Soc.* **2008**, *130*, 6940.
- (25) Gonzalez-Arellano, C.; Corma, A.; Iglesias, M.; Sanchez, F. *Chem. Commun.* **2005**, 1990.
- (26) Hoffmann-Röder, A.; Krause, A. *Org. Lett.* **2001**, *3*, 2537.
- (27) Haro, T.; Nevado, C. *J. Am. Chem. Soc.* **2010**, *132*, 1512.
- (28) Mizushima, E.; Sato, K.; Hayashi, T.; Tanaka, M. *Angew. Chem., Int. Ed.* **2004**, *41*, 4563.
- (29) Belting, V.; Krause, N. *Org. Biomol. Chem.* **2009**, *7*, 1221.
- (30) Suhre, M. H.; Reif, M.; Kirsh, S. F. *Org. Lett.* **2005**, *7*, 3925.
- (31) Mizushima, E.; Hayashi, T.; Tanaka, M. *Org. Lett.* **2003**, *5*, 3349.
- (32) Gross, Z.; Galili, N.; Simkhovich, L. *Tetrahedron Lett.* **1999**, *40*, 1571.
- (33) Yamada, M.; Kuzume, A.; Kurihara, M.; Kubo, K.; Nishihara, H. *Chem. Commun.* **2001**, 2476.
- (34) Ou, Z.; Kadish, K. M.; Wenbo, E.; Shao, J.; Sintic, P. J.; Ohkubo, K.; Fukuzumi, S.; Crossley, M. J. *Inorg. Chem.* **2004**, *43*, 2078.
- (35) Mullegger, S.; Schofderger, W.; Rashidi, M.; Reith, L. M.; Koch, R. *J. Am. Chem. Soc.* **2009**, *131*, 17740.
- (36) Eng, M. P.; Ljungdahl, T.; Andreasson, J.; Martensson, J.; Albensson, B. *J. Phys. Chem. A* **2005**, *109*, 1776.
- (37) Li, W.; Xie, Y.; Sun, R.-Y.; Liu, Q.; Young, J.; Yu, W.-Y.; Che, C.-M.; Tam, P. K.; Ren, Y. *Br. J. Cancer* **2009**, *101*, 342.
- (38) Zhou, C.-Y.; Chan, P. W. H.; Che, C.-M. *Org. Lett.* **2006**, *8*, 325.
- (39) Hashmi, A. S. K.; Schwarz, L.; Choi, H.; Frost, T. M. *Angew. Chem., Int. Ed.* **2000**, *39*, 2285.
- (40) Frisch, M. J.; et al. *Gaussian 03*; Gaussian, Inc.: Wallingford, CT, 2003.
- (41) Becke, A. D. *J. Chem. Phys.* **1993**, *98*, 5648.
- (42) Lee, C.; Yang, W.; Parr, R. G. *Phys. Rev. B* **1988**, *37*, 78.
- (43) Hay, P. J.; Wadt, W. R. *J. Chem. Phys.* **1985**, *82*, 299.
- (44) Hehre, W. J.; Radom, L.; Schleyer, P. v. R.; Pople, J. A. *Ab Initio Molecular Orbital Theory*; Wiley: New York, 1986.
- (45) Simon, S.; Duran, M.; Dannenberg, J. J. *J. Chem. Phys.* **1996**, *105*, 11024.
- (46) Barone, V.; Cossi, M.; Tomasi, J. *J. Comput. Chem.* **1998**, *19*, 404.
- (47) Barone, V.; Cossi, M.; Tomasi, J. *J. Comput. Chem.* **1998**, *19*, 404.
- (48) Takano, Y.; Houk, K. N. *J. Chem. Theory Comput.* **2005**, *1*, 70.
- (49) The allenone can, in principle, undergo a keto-enol tautomerism to form a *cis*-3-butyn-enol or *cis*-3-butyne-1-one, which can interact with the Au(III) center through the C≡C triple bond. However, B3LYP/6-31+G(d) calculations predict that both *cis*-3-butyn-enol and *cis*-3-butyne-1-one are higher in energy (by 18.1 kcal/mol (16.2 kcal/mol in acetone) and 9.8 kcal/mol (9.0 kcal/mol), respectively) than allenone, suggesting that such a mechanism will be unlikely.
- (50) Hashmi, A. S. K.; Ruppert, T. L.; Knöfel, T.; Bats, J. W. *J. Org. Chem.* **1997**, *62*, 7295.
- (51) Hargittai, M.; Schulz, A.; Reffy, B.; Kolonits, M. *J. Am. Chem. Soc.* **2001**, *123*, 1449.
- (52) Schulz, A.; Hargittai, M. *Chem.-Eur. J.* **2001**, *7*, 3657.
- (53) Dudnik, A. S.; Xia, Y.; Li, Y.; Gevorgyan, V. *J. Am. Chem. Soc.* **2010**, *132*, 7645.
- (54) Zhu, R.-X.; Zhang, D.-J.; Guo, J.-X.; Mu, J.-L.; Duan, C.-G.; Liu, C.-B. *J. Phys. Chem. A* **2010**, *114*, 4689.
- (55) Marshall, J. A.; Bartley, G. S. *J. Org. Chem.* **1994**, *59*, 7169.
- (56) Hashmi, A. S. K. *Chem. Rev.* **2007**, *107*, 3180.
- (57) Hashmi, A. S. K. *Catal. Today* **2007**, *122*, 211.
- (58) Benitez, D.; Shapiro, N. D.; Tkatchouk, E.; Wang, Y.; Goddard, W. A., III; Toste, F. D. *Nat. Chem.* **2009**, *1*, 482.
- (59) Fürstner, A.; Morency, L. *Angew. Chem., Int. Ed.* **2008**, *47*, 5030.
- (60) Hashmi, A. S. K. *Angew. Chem., Int. Ed.* **2008**, *47*, 6754.
- (61) Smith, M. B.; March, J. *March's Advanced Organic Chemistry: Reactions, Mechanisms, and Structure*, 6th ed.; Wiley-Interscience: New York, 2007.
- (62) Vives, A. C.; Arellano, C. G.; Corma, A.; Iglesias, M.; Sanchez, F.; Ujaque, G. *J. Am. Chem. Soc.* **2006**, *128*, 4756.
- (63) Lo, V. K.-Y.; Liu, Y.; Wong, M.-K.; Che, C.-M. *Org. Lett.* **2006**, *8*, 1529.